

## CERAMIC MEMBRANES IN HYBRID PHOTOCATALYSIS/ULTRAFILTRATION PROCESSES

**C.P. ATHANASEKOU<sup>1</sup>, N.G. MOUSTAKAS<sup>1</sup>, F.K. KATSAROS<sup>1</sup>, A.G. KONTOS<sup>1</sup>, G.E. ROMANOS<sup>1</sup>, S. MORALES-TORRES<sup>2</sup>, L.M. PASTRANA-MARTINEZ<sup>2</sup>, J.L. FARIA<sup>2</sup>, J.L. FIGUEIREDO<sup>2</sup>, A.M.T. SILVA<sup>2</sup>, C. FERNÁNDEZ-RODRÍGUEZ<sup>3</sup>, J.M. DONA-RODRIGUEZ<sup>3</sup> and P. FALARAS<sup>1</sup>**

<sup>1</sup>Division of Physical Chemistry, Institute of Advanced Materials, Physicochemical Processes, Nanotechnology and Microsystems (IAMPPNM), NCSR Demokritos, 15310 Aghia Paraskevi, Attikis, Athens, Greece

<sup>2</sup>LCM – Laboratory of Catalysis and Materials – Associate Laboratory LSRE/LCM, Faculdade de Engenharia, Universidade do Porto, Rua Dr. Roberto Frias, 4200-465 Porto, Portugal

<sup>3</sup>Grupo de Fotocatálisis y Espectroscopía Aplicada al Medioambiente-CIDIA. Dept. de Química Universidad De Las Palmas De Gran Canaria Campus Universitario de Tafira, 35017, Las Palmas de Gran Canaria, Spain  
e-mail: cathan@chem.demokritos.gr

### EXTENDED ABSTRACT

The current work demonstrates the efficiency of a hybrid Photocatalysis/Ultrafiltration process to eliminate or reduce the contents of synthetic dyes in wastewater. The process involves highly active photocatalytic ceramic ultrafiltration membranes prepared with the deposition of various photocatalysts on both sides of UF mono-channel monoliths. Anatase TiO<sub>2</sub> was deposited with chemical vapor deposition (CVD) and sol-gel (dip-coating) techniques. Novel materials such as modified TiO<sub>2</sub> with an organic shell layer and reduced graphene oxide-TiO<sub>2</sub> (rGO/TiO<sub>2</sub>) were also synthesised and stabilised on the surface and pore structure of the monoliths with the target to develop visible light responding membranes. The photocatalytic filtration experiments took place in a prototype water purification device in continuous flow conditions, using methylene blue (MB) and methyl orange (MO) as azo-dye model pollutants, under near-UV/Vis and visible light irradiation. The influence of several parameters, such as feed pressure, feed concentration and flow rate, on the pollutant degradation efficiency and membranes permeability was investigated and analysed. Furthermore, the novel hybrid process is compared with the standard Nanofiltration technique in regard to the pollutant removal efficiency and energy consumption.

**Keywords:** Ultrafiltration membranes; titanium dioxide; graphene oxide; azo-dye pollutants; photocatalysis; clean water.

### 1. INTRODUCTION

Advanced oxidation processes (AOPs) have been demonstrated as a viable alternative for the removal of organic pollutants showing environmental persistence from water and wastewater. Their behaviour towards degradation exhibits great advantages against the conventional biological treatment processes. AOP methods are characterized by the formation of OH<sup>•</sup> radicals onto the catalyst surface, which promote quantitative mineralization of a variety of organic pollutants to carbon dioxide and water. Nowadays, heterogeneous photocatalysis appears as one of the most destructive advanced

oxidation technologies for organic contaminants, being possible to obtain the complete mineralization of organic pollutants into CO<sub>2</sub>, water and inorganic ions, under ambient conditions and by using solar energy.

Titanium dioxide is a hot topic of research being very close to an ideal semiconductor for photocatalysis due to its high efficiency, stability, low cost and safety. After UV irradiation exceeding TiO<sub>2</sub> energy gap, electron-hole pairs are generated which favour redox reactions by formation of adsorbed radicals on the catalyst surface. However, practical application of TiO<sub>2</sub> photocatalytic materials is compromised by two inherent limitations, the recombination of photo-generated charge carriers, and the poor light-harvesting ability that is restricted by the wide band gap of TiO<sub>2</sub> to the UV spectral range (Likodimos *et al.*, 2010).

Towards the overcoming of these limitations novel modified TiO<sub>2</sub> catalyst have been developed and tested by the authors. The aim of the present work relies on the investigation of the parameters that govern the azo-dyes removal performance of these novel-titania based-photocatalysts when applied on ceramic ultrafiltration membranes as well as the comparison of the hybrid membranes produced with the NF used for water purification.

## 2. EXPERIMENTAL

### 2.1. Preparation of photocatalytic membranes

The dip-coating sols and the respective materials in powder form were prepared according to procedures previously described by the authors. More specifically, they have developed reduced graphene oxide-TiO<sub>2</sub> hybrids (GOT-4 and GOT-3.3) (Pastrana-Martínez *et al.*, 2012) and tested their photocatalytic activity under UV and VIS irradiation (Arana *et al.*, 2010). They have produced very efficient TiO<sub>2</sub> photocatalyst (ECT) from an ethanol, citric acid, titanium tetrabutoxide solution whereas (Moustakas *et al.*, 2013) developed VIS light active TiO<sub>2</sub>, modified with an organic shell layer (N-TiO<sub>2</sub>), via a nitric acid acidified tetrabutyl orthotitanate solution. The deposits were developed on  $\gamma$ -alumina UF cylindrical membrane substrates (mono-channel tubes) possessing glazed ends of 1.5 cm length, provided by Fraunhofer IKTS (Fraunhofer Institute for Ceramic Technologies and Systems, Germany) under the commercial name of Inopor<sup>®</sup>. They presented nominal pore size of 5 nm and 10nm, and had a length of 15 cm, ID and OD of 7 and 10 mm, respectively. In addition to the dip-coating technique two different Chemical Vapour Deposition methods were also applied for the photocatalytic membranes development.

CVD 5nm membranes. The first CVD method involved pyrolytic decomposition of titanium tetrakisopropoxide (TTIP) vapor and formation of TiO<sub>2</sub> nanoparticles through homogeneous gas phase reactions and aggregation of the produced intermediate species (Romanos *et al.*, 2012). The grown nanoparticles diffused and deposited on the surface of  $\gamma$ -alumina 5-nm membrane tubes.

CVD 10nm membranes. The second CVD method proceeded through layer-by-layer deposition (LBL) of TiO<sub>2</sub> and comprised chemisorption or physisorption of the titanium isopropoxide (TTIP) vapour and a subsequent oxidative treatment in order to promote the precursor condensation and generate new adsorption sites for the accomplishment of the successive adsorption/surface reaction steps (Athanasakou *et al.*, 2012).

N-TiO<sub>2</sub> 5nm membranes. The  $\gamma$ -Al<sub>2</sub>O<sub>3</sub> (5 nm) membranes were coated with the HNO<sub>3</sub> acidified sol using the dip-coating technique. The glazing at both ends was covered with Teflon tape and then the membrane was dipped into the sol in a vertical position following three successive dip in – pull out cycles at a rate of 15 cm min<sup>-1</sup>. The purpose was to deposit the organic shell layer modified TiO<sub>2</sub> catalyst on the inner and outer surface of the

tubular membrane simultaneously as well as on the intermediate pores, in order to enhance the pollutants photodegradation efficiency by illuminating both membrane surfaces during the filtration process. The membrane was heated at a rate of 0.5 °C/min to 400 °C, where it remained for 2 hours. The prepared membranes were weighted after calcination and were found heavier by 20 mg (0.033 mg/cm<sup>2</sup>).

GOT 10nm membranes. The  $\gamma$ -Al<sub>2</sub>O<sub>3</sub> membranes (10 nm) were coated with the hybrid rGO/TiO<sub>2</sub> photocatalyst using the liquid phase deposition method at room temperature. The glazing at both ends was covered with Teflon tape and then the membrane was dipped into the sol in a vertical position following successive dip in – pull out cycles. The membrane was heated at a rate of 0.5 °C/min to 200 °C, where it remained for 2 hours. Bare TiO<sub>2</sub> was also prepared by using the same method but without addition of graphene oxide and treated at 200 °C.

ECT 10nm membranes. These catalysts were synthesized following a sol–gel procedure of the solution described in paragraph 2.1. The high photocatalytic efficiency of ECT calcined at 750°C is related to its enhanced availability to originate reactive hydroxyl radicals from photoinduced holes at the catalyst surface.

## 2.2. The photocatalytic membrane reactor

The photocatalytic activity of the developed TiO<sub>2</sub> membranes in flow-through mode was evaluated in terms of MO and MB dye decomposition in a continuous flow water purification device, applying UV irradiation on both membrane sides. The photocatalytic membrane reactor comprises a fluid delivery system, the reactor cell, the irradiation sources, a pressure transducer, and a backpressure regulator. It works at pressures up to 20 bars. The UV irradiation external surface was at the near-UV area (315–380 nm) with a peak at 365 nm and a light intensity of 2.1 mW cm<sup>-2</sup>. The UV irradiation of the internal surface was, as well, at the near-UV radiation area (360–420 nm) with a peak at 383–392 nm and at a light intensity of 0.5 mW cm<sup>-2</sup>. The visible irradiation of the external surface had a light intensity 7.2 mW cm<sup>-2</sup>, while the visible irradiation of the internal surface had a peak at 460 nm at a light intensity of 0.3 mW cm<sup>-2</sup>. More technical characteristics and figures of the reactor have been published by the authors elsewhere (Papageorgiou *et al.*, 2012).

## 3. Results and Discussion

### 3.1. Surface characterisation and Sorption Capacity of the materials

The sorption capacity of the three photocatalysts applied on the membranes via the sol gel procedure (ECT, N-TiO<sub>2</sub>, GOT4), was tested with batch sorption experiments. As shown in

Figure 1 the N-doped and the ECT titania powders exhibit a preference to MB, compared to MO and their MO uptake is similar to this of the GOT4 powder. The surprisingly high value of MO sorption capacity onto GOT4 cannot be explained in terms of its high BET surface area (**Error! Reference source not found.**).

**Table 1.** Surface area defined by Liquid Nitrogen porosimetry.

Catalyst	P25	ECT	N-TiO <sub>2</sub>	GOT-4
S <sub>BET</sub> (m <sup>2</sup> g <sup>-1</sup> )	52	18	141	117

As seen, both N-TiO<sub>2</sub> and GOT4 powders exhibit high BET values compared to ECT and Degussa P25. Thereby the higher MO adsorption capacity can be attributed to the selective adsorption of MO on the reduced graphene oxide.

### 3.2. Activity of the photocatalysts in powder form

The effectiveness of the three photocatalysts applied on the membranes via the sol gel procedure (ECT, N-TiO<sub>2</sub>, GOT3.3), was evaluated in batch experiments for the degradation of methyl orange (MO, 3.05×10<sup>-5</sup> mol L<sup>-1</sup>) in aqueous solutions under UV and VIS light irradiation. The results obtained with MO are presented in Figure 2.

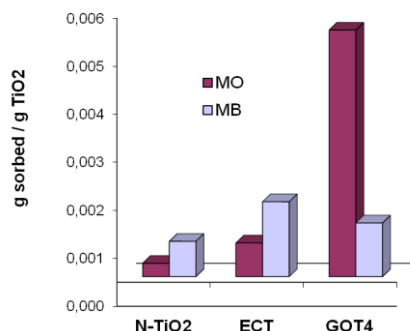


**Figure 1.** Pollutant sorption capacity of the three powder-like-form catalysts.

Significant enhancement of the photocatalytic activity has been frequently observed when rGO is combined with TiO<sub>2</sub>, due to their synergetic interaction encompassing both interfacial electron transfer between the two constituent phases and the markedly enhanced adsorption capacity of rGO for pollutant molecules. At tested conditions, the composite prepared with TiO<sub>2</sub> and reduced graphene oxide (GOT) exhibited the highest activity under UV irradiation, which can be attributed to the optimal assembly and interfacial coupling between the graphene oxide sheets and TiO<sub>2</sub> nanoparticles, allowing graphene oxide to generate more reactive radicals than the respective bare TiO<sub>2</sub> material via the reaction of stored and transported electrons from UV irradiated TiO<sub>2</sub>.

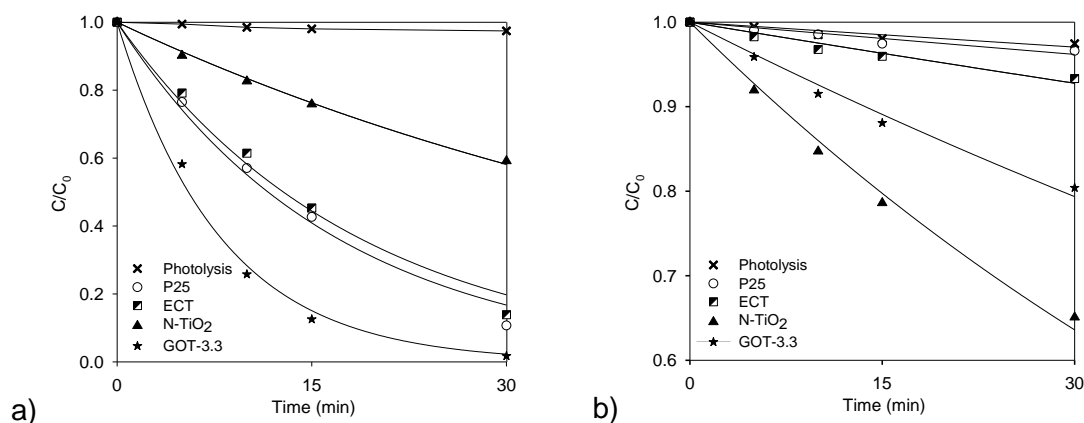


**Figure 2:** Photocatalytic degradation of MO (10 mg L<sup>-1</sup>) over P25, ECT, N-TiO<sub>2</sub> and GOT-3.3 under a) near-UV b) visible light irradiation. Catalyst load = 0.5 g L<sup>-1</sup>. Curves represent the fitting of the pseudo-first order equation to the experimental data.

On the other hand, N-doped TiO<sub>2</sub> presented better photocatalytic activity under visible light illumination. The nitrogen-doped photocatalysts has the highest shift of the energy band gap to the visible range ( $E_g = 2.23$  eV) due to the introduction of nitrogen at

interstitial lattice sites of  $\text{TiO}_2$ , suggesting at this point that the N- $\text{TiO}_2$  catalysts could be the most efficient photocatalyst, at least under visible light illumination. Therefore, both GOT and ECT are efficient materials for photocatalytic reactions under near-UV/Vis irradiation, while GOT and N- $\text{TiO}_2$  seem to be more appropriate for visible ( $\lambda > 430 \text{ nm}$ ) light applications. Previous studies using ECT as catalyst and MO as model pollutant show that the high efficiency of ECT is attributed to the enhanced formation of reactive hydroxyl radicals at the catalyst surface. All the prepared photocatalysts present a narrowed band-gap than Degussa P25 ( $E_g = 2.97, 2.95, 2.28$  and  $3.18 \text{ eV}$  for ECT, GOT, N- $\text{TiO}_2$  and P25, respectively). This is a clear indication that the activation mechanisms are different for each material, but GOT is able to switch between the more appropriate pathways defining on excitation. In fact, composites based on graphene oxide and  $\text{TiO}_2$  are already shown in literature to be highly active photocatalysts for different azo dyes. The GOT composite may effectively enhance the photocatalytic activity of  $\text{TiO}_2$  in the visible range without compromising the performance under UV irradiation, a major drawback usually associated to visible light active anion doped  $\text{TiO}_2$  photocatalysts. The photocatalytic activity of the prepared composites was Values of  $k$  presented in Table 2 are obtained considering the pseudo-first order kinetic model ( $C = C_0 e^{-kt}$ ).

**Table 2.** Pseudo first-order kinetic rate constant ( $k$ ) and regression coefficient ( $r^2$ ) of MO degradation under UV and visible irradiation at different conditions.

	UV		Vis	
	$k \times 10^{-3} \text{ (min}^{-1}\text{)}$	$r^2$	$k \times 10^{-3} \text{ (min}^{-1}\text{)}$	$r^2$
Photolysis	1.00	0.92	n.d.	n.d.
P25	51.5	0.98	4.50	0.96
$\text{TiO}_2$ reference to GOT	3.00	0.99	1.00	0.98
GOT3.3	102	0.995	4.30	0.993

### 3.3. Ultrafiltration with simultaneous Adsorption and Photocatalysis

In order to evaluate the membranes efficiency in removing MO and MB, filtration experiments with simultaneous photocatalysis and adsorption took place under UV irradiation. Prior to each of the experiments, the pollutant solution was oxygenated for 2h and was used to fill the reactor's piston (0.6 L capacity). The main parameters determined during each test were: a) the time required to collect 10 ml of treated permeate, b) the transmembrane pressure inside the cell, c) the pollutant concentration in each sample collected. The photocatalytic tests were performed in the flow-through filtration mode, since our intention was to test the developed membranes under fouling prone conditions.

Figure 3 show the amount of pollutant removed vs the amount of pollutant introduced into the reactor cell, for each of the tested membranes.

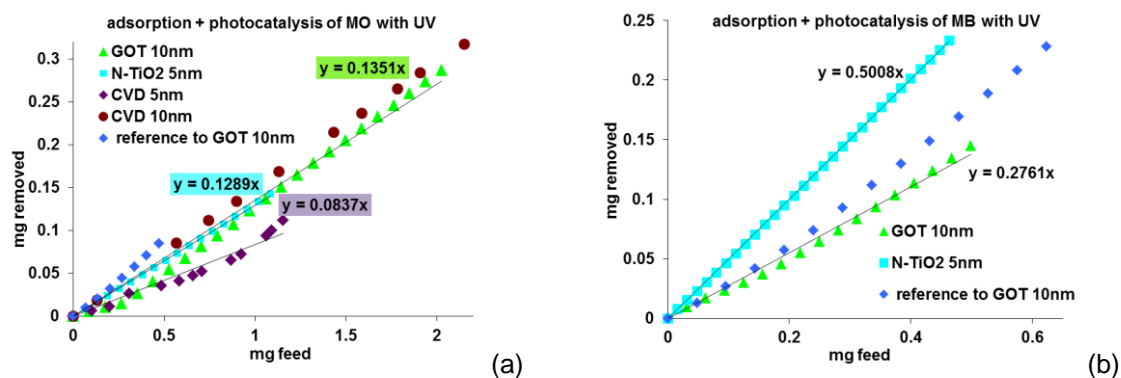


**Figure 3.** Results of flow experiments through the catalyst-modified membranes under UV irradiation. Total flow: 1.5 ml/min, pollutant feed concentration a) MO 6.4 mg/L b) MB 2 mg/L

### 3.4. Ultrafiltration Photocatalysis experiments

To eliminate the effect of sorption and define the hybrid UF/photocatalytic efficiency of the membranes, the filtration experiments proceeded initially in dark until equalization of the concentration of the pollutant in the permeate with this in the feed solution. Then irradiation was applied and the results are showed in Figure 5 and Figure 6.

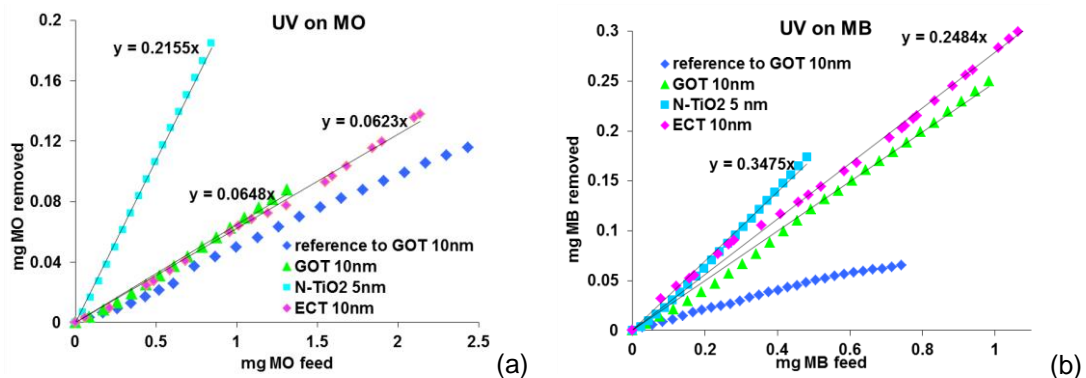


**Figure 5.** Results of flow experiments through the catalyst-modified membranes under UV irradiation. Total flow: 1.5 ml/min, pollutant feed concentration a) MO 6.4 mg/L b) MB 2 mg/L

The slope of the treadline fitted to the points represents the photocatalytic efficiency of each membrane. Comparison between the efficiencies presented in Figures 4 and 5 reveal the considerable effect of sorption. Under UV irradiation, the N-TiO<sub>2</sub> 5nm membrane is the most efficient of all against MO and MB. The graphene oxide addition to TiO<sub>2</sub> seems to enhance the degradation efficiency for both pollutants. All the developed membranes performed much better against MB than MO. The organic shell layer modification of the TiO<sub>2</sub> catalyst attempts to activate it in the visible light area via the formation of localized energy states within titania's band gap. This was confirmed by the results of the experiments using MB as pollutant (Figure b), while the experiments with MO exhibited an efficiency level even lower of those of the ECT and GOT membranes.

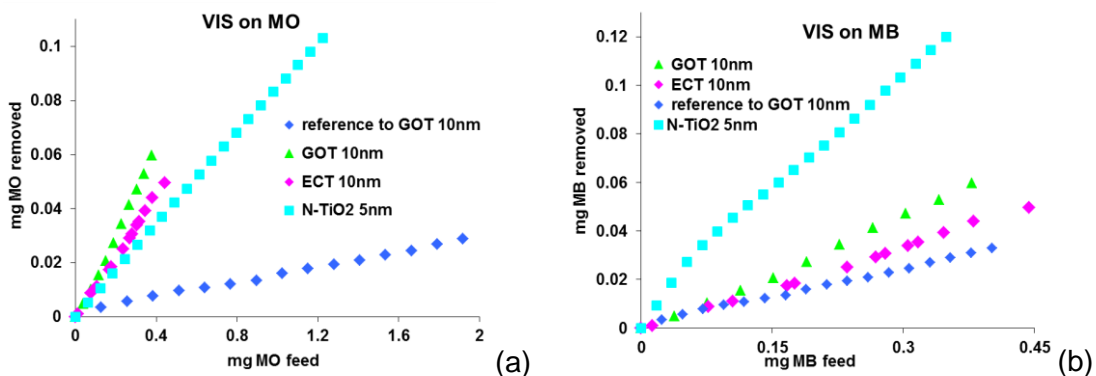


**Figure 6.** Results of flow experiments through the catalyst-modified membranes under VIS irradiation. Total flow: 1.5 ml/min, pollutant feed concentration a) MO 6.4

mg/L b) MB 2 mg/L

Synergetic effects between rGO and TiO<sub>2</sub> are revealed by the higher photocatalytic efficiency of membrane GOT 10nm for MO under VIS irradiation. As described in the following table the N-TiO<sub>2</sub> has a band gap of 2.28eV which is the smallest of the ones of the tested materials.

**Table 3.** The band gap of the photocatalysts used for the development of membranes.

Catalyst	P25	ECT	N-TiO <sub>2</sub>	GOT4
Eg (eV)	3.18	2.97	2.28	2.95
Maximum Wavelength (*)	389.9	417.5	543.8	420.3

As a result the N-TiO<sub>2</sub> photocatalyst can efficiently harvest photons of larger wavelengths thus exploiting wider part of the solar spectrum.

### 3.5. Comparison with commercial NF membranes

Table 4 presents the performance characteristics (regarding dyes rejection) of the developed membranes in comparison with those of commercially available (TFC) polymeric nanofiltration membranes. The comparison take place in terms of a) the trans-membrane pressure applied, b) the %water recovery values, c) the water permeance d) the % pollutant rejection values e) energy consumption.

**Table 3.** Performance of the developed membranes compared to that of commercially available, thin film composite nanofiltration polymeric membranes (TFC-NF)

	Conc. mg/L (MB-MO)	Pressure bar	Water Recovery %	Feed flow (L/h)	Permeance per square meter (L/h)	R %	kWh
N-TiO <sub>2</sub>	2-6.5	2.5	100	33.3	33.3	45-65	0.07
GOT	2-6.5	2	100	34	34	45	0.05
CVD 5 nm	2-6.5	14	28	17.03	4.77	55-60	0.4
CVD 10nm	2-6.5	2.5	90	45	40	15	0.07
MSP 31 Weizmann NF 45	400-500	25	80	83	66.25	94.9	0.9
Dow/Film Tec	400-500	25	80	49	39.2	92	0.9
DK 1073 Osmonics	400-500	25	80	75	60.25	94.5	0.9
TFC-SR2 Fluid System	92-1580	5	80	56	45.05	97.7	0.2
NTR 7450 Nitto-Denko	1000	20	80	80	64	92.1	0.7
Desal 5 DK Osmonics	500-2000	10	80	52	41.1	100	0.35

The energy consumption (kWh) was calculated in terms of the pump power (shaft power) over the time needed to drive 1m<sup>3</sup> of water to the membrane module, overcoming in parallel the pressure drop generated on the opposite sides of the membrane during the cross flow filtration. It was calculated by means of following equation:

$$E(\text{kWh}) = 100 \times \frac{P \times \rho_w}{S \times 36}$$

where  $P$  (bar) the pressure in the retentate side of the membrane,  $\rho_w$  ( $\text{g/cm}^3$ ) the density of the fluid and  $S$  the pump efficiency (usually 0.8). The energy consumption comparison is made on the basis of the treatment of  $1 \text{ m}^3$  of water (permeate) by  $1 \text{ m}^2$  of active membrane surface. Moreover compared to the commercial TFC-NF membranes, the developed membranes exhibited almost one third of the rejection efficiency, but about 1.3 times higher water recovery. Most of the developed membranes (GOT, N-TiO<sub>2</sub>, ECT and CVD 10nm) operated at extremely low energy consumption which is about 10-12 times lower than this required by the commercial NF membranes. Thereafter, by recycling the permeate effluent of the developed membranes back to the feed, we need about 3 times higher treatment period to achieve the rejection efficiency of a TFC-NF membrane. In general, compared to TFC-NF, the developed high flux photocatalytically active membranes have the capacity to treat identical volume of polluted water and bring it at similar quality expensing 7 times lower energy.

## 5. CONCLUSIONS

Photocatalytic ceramic membranes have been developed and their efficiency for MO and MB removal from water was tested in filtration units involving UV or VIS irradiation on both membrane sides. The membranes were proved very efficient and compared to standard NF membranes they could remove the same amount of pollutant with lower energy consumption and no production of concentrated effluents.

## REFERENCES

1. Arana J., Dona-Rodríguez J.M., Portillo-Carrizo D., Fernández-Rodríguez C, Pérez-Pena J., González Díaz O., Navío J.A. and Macías M. (2010), Photocatalytic degradation of phenolic compounds with new TiO<sub>2</sub> catalysts, *Appl. Catal., B*, **100**, 346-354.
2. Athanasekou C.P., Romanos G.E., Katsaros F.K., Kordatos K., Likodimos V. and Falaras P. (2012), Very efficient composite titania membranes in hybrid ultrafiltration/photocatalysis water treatment processes, *J. Membrane Sci.*, **392-393**, 192-203.
3. Likodimos V., Dionysiou D. and Falaras P. (2010), CLEAN WATER: water detoxification using innovative photocatalysts, *Rev Environ Sci Biotechnol.*, **9**, 87-94.
4. Moustakas N.G., Kontos A.G., Likodimos V., Katsaros F., Boukos N., Tsoutsou D., Dimoulas A., Romanos G.E., Dionysiou D.D. and Falaras P. (2013), Inorganic–organic core–shell titania nanoparticles for efficient visible light activated photocatalysis, *Appl. Catal., B*, **130-131**, 14-24.
5. Papageorgiou S.K., Katsaros F.K., Favvas E.P., Romanos G. Em., Athanasekou C.P., Beltsios K.G., Tziaila O.I. and Falaras P. (2012), Alginate fibers as photocatalyst immobilizing agents applied in hybrid photocatalytic/ultrafiltration water treatment processes, *Water Res.*, **46**, 1858-1872.
6. Pastrana-Martínez L. M., Morales-Torres S., Likodimos V., Figueiredo J.L., Faria J.L., Falaras, P. and Silva, A.M.T. (2012), Advanced nanostructured photocatalysts based on reduced graphene oxide-TiO<sub>2</sub> composites for degradation of diphenhydramine pharmaceutical and methyl orange dye, *Appl. Catal., B*, **123-124**, 241-256.
7. Romanos G.Em., Athanasekou C.P., Katsaros F.K., Kanellopoulos N.K., Dionysiou D.D., Likodimos V. and Falaras P. (2012), Double-side active TiO<sub>2</sub>-modified nanofiltration membranes in continuous flow photocatalytic reactors for effective water purification, *J. Hazard. Mater.*, **211-212**, 304-316.